

Effects of sintering time on crystal structure, dielectric properties and conductivity of $(\text{Ca}_{0.8}\text{Sr}_{0.2})\text{ZrO}_3$ ceramics

Weina Chen · Huiqing Fan · Changbai Long ·
Shenhui Lei

Received: 5 December 2013 / Accepted: 22 January 2014 / Published online: 30 January 2014
© Springer Science+Business Media New York 2014

Abstract $(\text{Ca}_{0.8}\text{Sr}_{0.2})\text{ZrO}_3$ ceramics were prepared using solid-state reaction process, which were sintered at 1,480 °C for different sintering time (2, 4, 6, 8, 10, 12 h, respectively), their structures were characterized by X-ray diffraction (XRD), scanning electron microscopy, transmission electron microscopy and Raman spectroscopy. Rietveld refinement for the $(\text{Ca}_{0.8}\text{Sr}_{0.2})\text{ZrO}_3$ sintered for 10 h was carried out by powder XRD at room temperature and it crystallizes in orthorhombic space group *Pnma* [$a = 5.77341(4)$ Å, $b = 8.05569(6)$ Å, $c = 5.63318(4)$ Å and $V = 261.9920(30)$ Å³, $Z = 4$]. The $(\text{Ca}_{0.8}\text{Sr}_{0.2})\text{ZrO}_3$ ceramics sintered at 1,480 °C for 2–12 h possessed a dielectric constant (ϵ_r) of 23.6–27.9, a quality factor ($Q \times f$) of 2,160–21,460 GHz and a temperature coefficient of resonant frequency (τ_f) from –14 to +13.6 ppm/°C. The Arrhenius plot of the dc electrical conductivity changed significantly with increasing sintering time.

1 Introduction

Dielectric materials have been studied for decades due to both their application in important technologies and the fundamentally interesting relationships among their crystal chemistry, crystal structure and physics properties. Owing to a significant development in microelectronics, especially, wireless communications technologies, it is necessary to find some microwave dielectric materials, which possess high dielectric constant, low dielectric loss and

near-zero temperature coefficient of resonant frequency [1]. High dielectric constant can effectively reduce the size of resonators, and the dielectric loss must be low to achieve prominent frequency selectivity and stability in microwave transmitter components. Moreover, a small temperature coefficient of resonant frequency is needed to ensure the stability of the microwave components at different working temperatures. However, in practice, high dielectric constant materials, exhibit high dielectric loss (low $Q \times f$ value) and large positive τ_f value, whereas low loss ceramics are usually accompanied by low ϵ_r value and negative τ_f value [2]. The most convenient and promising way to achieve a zero τ_f value is to combine two or more compounds with negative and positive temperature coefficients to form homogeneous solid solution or inhomogeneous mixtures with low temperature coefficients [3].

CaTiO_3 and SrTiO_3 have been individually employed as an effective τ_f compensator to materials having negative τ_f , such as MgTiO_3 , Mg_2TiO_4 , $\text{Mg}_4\text{Nb}_2\text{O}_9$, $\text{La}(\text{Zn}_{1/2}\text{Ti}_{1/2})\text{O}_3$, $(\text{Mg}_{0.95}\text{Co}_{0.05})_2\text{TiO}_4$ and $\text{Ca}(\text{Mg}_{1/3}\text{Ta}_{2/3})\text{O}_3$ [1, 4]. Wise et al. [5] reported that the $(\text{Ca}_{0.8}\text{Sr}_{0.2})\text{TiO}_3$ ceramics have a ϵ_r of 181, a τ_f of 991 ppm/°C and a $Q \times f$ of 8,300 GHz which is much higher than those of pure CaTiO_3 and SrTiO_3 . Also, many works proved that $(\text{Ca}_{0.8}\text{Sr}_{0.2})\text{TiO}_3$ exhibits perfect advantages as an τ_f compensator [6]. For CaTiO_3 based materials, the substitution at the A site is proposed to be an effective way to improve their dielectric properties [7]. In addition, CaZrO_3 and SrZrO_3 [8] have the same simple (perovskite) structure as many titanate compounds. Perovskite materials readily form homogeneous and reproducible solid solutions with wide ranges of properties.

In the present work, $(\text{Ca}_{0.8}\text{Sr}_{0.2})\text{ZrO}_3$ ceramics were prepared by solid-state reaction process, where Zr^{4+} fully substitution for Ti^{4+} at B site in $(\text{Ca}_{0.8}\text{Sr}_{0.2})\text{TiO}_3$. They

W. Chen · H. Fan (✉) · C. Long · S. Lei
State Key Laboratory of Solidification Processing, School of
Materials Science and Engineering, Northwestern Polytechnical
University, Xi'an 710072, People's Republic of China
e-mail: hqfan3@163.com

were sintered at 1,480 °C for 2 h (CSZ-2), 4 h (CSZ-4), 6 h (CSZ-6), 8 h (CSZ-8), 10 h (CSZ-10), 12 h (CSZ-12), respectively. The dielectric properties both in microwave frequency and low frequency (100 Hz–1 MHz), crystal structure and conductivity were studied in detail.

2 Experimental procedure

(Ca_{0.8}Sr_{0.2})ZrO₃ ceramics were prepared through a conventional mixed oxide route from the high-purity raw powders of CaCO₃ (99.9 %), SrCO₃ (99.9 %) and ZrO₂ (99.9 %). Stoichiometric proportions of (Ca_{0.8}Sr_{0.2})ZrO₃ were mixed by a ball milling method in ethanol for 12 h. The mixtures were dried at 80 °C and then calcined at 1,150 °C for 4 h. The calcined powder was remilled in ethanol for 12 h, dried, ground, and cold isostatically pressed into pellets with a diameter of 12 mm and a thickness of 6 mm at 200 MPa. The pressed pallets were then sintered at 1,480 °C with the heating and cooling rate of 5 °C/min for 2, 4, 6, 8, 10 and 12 h, respectively.

Densities of all samples were measured by the Archimedes method. Powder X-ray diffraction (XRD) data were obtained by using an automated diffractometer (X'Pert PRO MPD, Philips, Eindhoven, The Netherlands) with a nickel filter (Cu K α radiation) at room temperature. Raman spectra of the samples were performed with an instrument (LabRAM HR800, Horiba Jobin-Yvon, Lyon, France) in a backward scattering geometry. Lattice images were obtained by a transmission electron microscopy (TEM; TecnaiF30, FEL, Hillsboro, OR, USA) operated at 300 kV accelerating voltage. Surface morphologies were observed using scanning electron microscopy (SEM; S-570, Hitachi, Tokyo, Japan). The sintered pellets were polished to a final thickness of 1 mm and then were coated with silver electrodes for electrical measurements. Variable-temperature dielectric properties in the range of 100 Hz–1 MHz were measured by a precision impedance analyzer (4294A, Agilent, Santa Clara, CA) with temperature controller (TP94, Linkam, Surrey, UK) at the heating rate of 2 °C/min. A high resistance meter (4339B, Agilent, Santa Clara, CA) was employed to measure dc conductivities of the samples. Dielectric constant (ϵ_r) and quality factor values (Q) in the range of microwave frequencies were measured using the Hakki and Coleman's dielectric resonator method [9, 10], with a system combining a network analyzer (8720E, Agilent, Santa Clara, CA). The temperature coefficients of resonant frequency τ_f values were calculated by the formula as following:

$$\tau_f = \frac{f_T - f_0}{f_0(T - T_0)} \quad (1)$$

where f_T , f_0 are the resonant frequencies at the measuring temperature T (85 °C) and T_0 (25 °C), respectively.

3 Results and discussion

XRD patterns of the (Ca_{0.8}Sr_{0.2})ZrO₃ ceramics with different sintering time are shown in Fig. 1, the result reveals that there do not exist any second phase, and all the diffraction peaks can be indexed to the perovskite CaZrO₃ with orthorhombic space group *Pnma* (62) (ICSD-PDF #35-0790; $a = 5.756$ Å, $b = 8.010$ Å, $c = 5.593$ Å). The calculated lattice parameters a , b , and c all ceramics are listed in Table 1. An increase in sintering time leads to a decrease in a and c and an increase in b . Correspondingly, the cell volumes of the (Ca_{0.8}Sr_{0.2})ZrO₃ ceramics decreased gradually with increasing sintering time, which could be attributed to the oxygen loss due to long-time high temperature sintering.

Figure 2 shows that Raman spectra of all samples from 100 to 600 cm⁻¹ at room temperature. It is observed that the peak positions remain unchanged while the width of the mode decreased with increasing time. All Raman spectra exhibits intense phonon modes at 190, 234, 274, 343, 430 and 543 cm⁻¹, which are related to orthorhombic phase and similar to the reported by Orera et al. [11], The modes

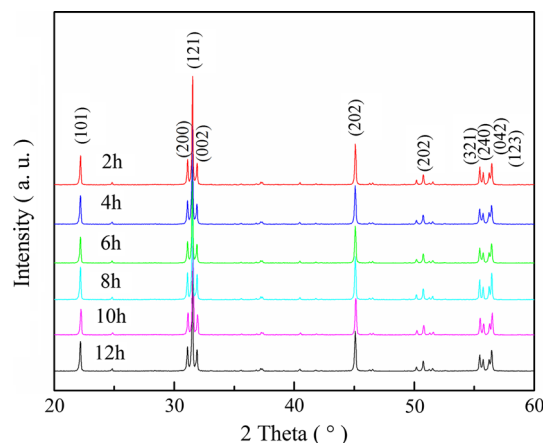


Fig. 1 XRD patterns of (Ca_{0.8}Sr_{0.2})ZrO₃ ceramics sintered at 1,480 °C for 2–12 h

Table 1 Lattice parameters and cell volumes of the (Ca_{0.8}Sr_{0.2})ZrO₃ ceramics sintered at 1,480 °C for 2–12 h

| Sintering time (h) | Lattice parameters (Å) | | | Cell volumes (Å ³) | Space group (PDF#35-0790) |
|--------------------|------------------------|--------|--------|--------------------------------|---------------------------|
| | a | b | c | | |
| 2 | 5.7695 | 8.0708 | 5.6378 | 262.5212 | <i>Pnma</i> (62) |
| 4 | 5.7653 | 8.0756 | 5.6180 | 261.5643 | |
| 6 | 5.7564 | 8.0802 | 5.6177 | 261.2953 | |
| 8 | 5.7560 | 8.0813 | 5.6152 | 261.1964 | |
| 10 | 5.7528 | 8.0833 | 5.6113 | 260.9345 | |
| 12 | 5.7506 | 8.0963 | 5.6025 | 260.8445 | |

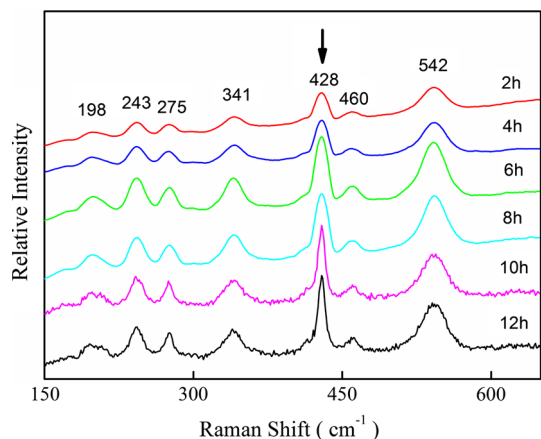


Fig. 2 Raman spectra from 100 to 650 cm^{-1} at room temperature

at 190, 234, 274 and 343 cm^{-1} are associated with oxygen octahedral rotation while the 430 and 543 cm^{-1} modes are related to the torsion and stretch of Zr–O bond, respectively [12, 13]. The width of the mode decreased with increasing sintering time implying that the arrangement of atoms in crystal became more orderly.

In order to characterize structures of the prepared oxides, XRD Rietveld refinement for the CSZ-10 ceramics was carried out with *Pnma* space group at room temperature, using the GSAS–EXPGUI program [14, 15]. The XRD data were collected in the range of 10° – 130° with a step size of 0.017° . The coordinates of $(\text{Ca}_{0.97}\text{Li}_{0.03})(\text{Ta}_{0.03}\text{Zr}_{0.97})\text{O}_3$ were used as an initial model where Ca (80 %) and Sr (20 %) occupied the $(\text{Ca}_{0.97}\text{Li}_{0.03})$ (4a) site and the $(\text{Ta}_{0.03}\text{Zr}_{0.97})$ (4b) site was fully occupied by Zr (100 %). The final refined profile for CSZ-10 is shown in Fig. 3a. The summary of crystallographic data, *R* factors and experimental conditions is listed in Table 2. The final factors, R_{wp} , R_p and Chi squared values (χ^2) for CSZ-10 are 5.41, 4.01 and 2.525 %, respectively. These values are reasonable and it suggests that the prepared CSZ-10 crystallizes in orthorhombic space group, *Pnma* [$a = 5.77341(4)$ Å, $b = 8.05569(6)$ Å, $c = 5.63318(4)$ Å and $V = 261.9920(30)$ Å³; $Z = 4$]. Comparing to those of $(\text{Ca}_{0.97}\text{Li}_{0.03})(\text{Ta}_{0.03}\text{Zr}_{0.97})\text{O}_3$ [16], an increase in *a*, *b* and *c* is observed for CSZ-10, which should be contributed to the replacement of A-site Ca^{2+} [1.34 Å, 12 coordination number (CN)] by larger size Sr^{2+} (1.44 Å, 12 CN) [17]. The atomic coordinates, atomic occupancies and isotropic thermal parameters of the CSZ-10 are listed in Table 3. On the basis of the refined results, the crystal structure of CSZ-10 along [001], [101] and [100] directions at room temperature is depicted in Fig. 3b.

Figure 4 shows a high-resolution transmission electron microscopy (HRTEM) image of the CSZ-10 viewed along the [010] zone-axis. The periodic fringes are clearly

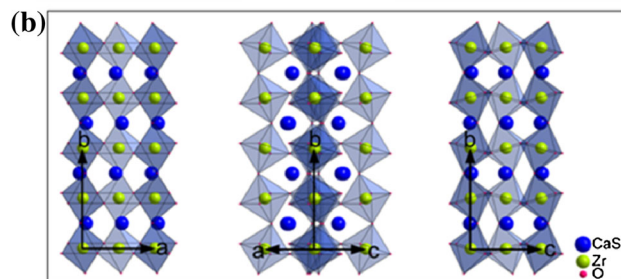
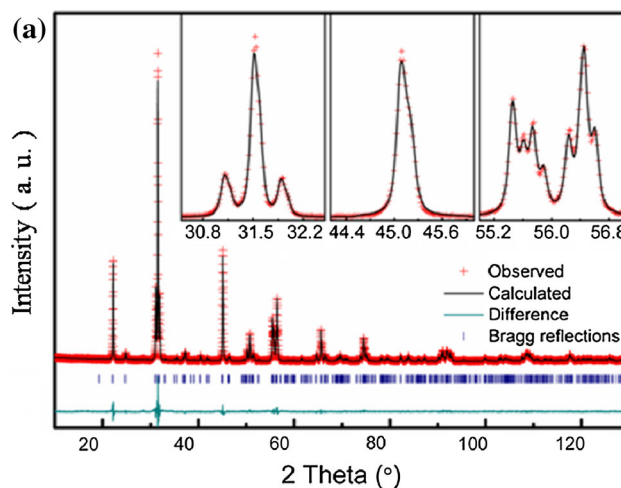


Fig. 3 **a** Rietveld refinement of the $(\text{Ca}_{0.8}\text{Sr}_{0.2})\text{ZrO}_3$ ceramics sintered at $1,480^\circ\text{C}$ for 10 h. **b** Refined crystal structure of $(\text{Ca}_{0.8}\text{Sr}_{0.2})\text{ZrO}_3$ ceramics sintered for 10 h viewed along [001], [101] and [100] directions

Table 2 Crystal data and structure refinement conditions for CSZ-10

| Compound reference | CSZ-10 |
|--|--|
| Chemical formula | $(\text{Ca}_{0.8}\text{Sr}_{0.2})\text{ZrO}_3$ |
| Formula mass | 188.81 |
| Crystal system | Orthorhombic |
| <i>a</i> (Å) | 5.77341(4) |
| <i>b</i> (Å) | 8.05569(6) |
| <i>c</i> (Å) | 5.63318(4) |
| Unit cell volume (Å ³) | 261.9920(30) |
| Temperature (K) | 298 |
| Space group | <i>Pnma</i> |
| No. of formula units per unit cell, <i>Z</i> | 4 |
| No. of reflections | 482 |
| No. of data points | 7,059 |
| Reduced χ^2 | 2.525 |
| R_{wp} (%) | 5.45 |
| R_p (%) | 4.01 |

observed, with a spacing of about 0.8 nm equivalent to the lattice parameter *b*, 0.805569(6) nm. The corresponding selected area electron diffraction (SAED) pattern recorded

Table 3 Atomic coordinates, atomic occupancies and isotropic thermal parameters of the CSZ-10 at room temperature

| Atom | Site | x | y | z | $100U_{\text{iso}} (\text{\AA}^2)$ | Occupancy |
|------|------|--------------|------------|-------------|------------------------------------|-----------|
| Ca1 | 4a | 0.04297 (19) | 0.25 | −0.0083 (4) | 0.741 (26) | 0.8 |
| Sr1 | 4a | 0.04297 (19) | 0.25 | −0.0083 (4) | 0.741 (26) | 0.2 |
| Zr1 | 4a | 0 | 0 | 0.5 | 0.324 (10) | 1 |
| O1 | 4a | −0.0320 (9) | 0.25 | 0.4034 (8) | 0 | 1 |
| O2 | 8b | 0.2968 (6) | 0.0520 (4) | 0.7021 (6) | 0 | 1 |

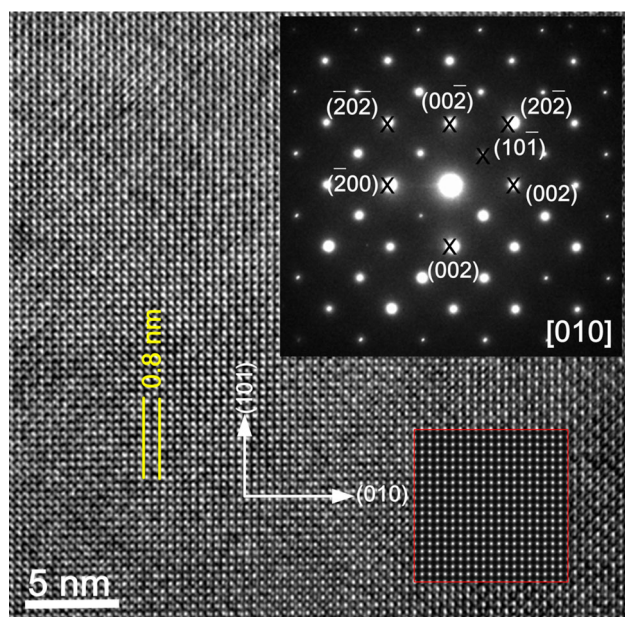


Fig. 4 HRTEM image of the $(\text{Ca}_{0.8}\text{Sr}_{0.2})\text{ZrO}_3$ ceramics sintered at 1,480 °C for 10 h. Insets show the [010] zone-axis SAED pattern and HRTEM image simulation (calculation parameters: crystal thickness = 1 nm; defocus value = −10 nm)

along the [010] zone axis is shown in the inset of Fig. 4. Superstructure reflections arising from the unit cell doubling are probably present in CSZ-10 and the patterns can be indexed according to an A-centered orthorhombic cell ($Pnma$) with the refined lattice parameters. Furthermore, with the crystallographic data of the refined structure, HRTEM image simulation for the CSZ-10 was performed with the *Jems* program using the Blochwave method [18]. The inset of Fig. 4 shows a fair agreement between experimental and calculated contrasts at a crystal thickness of 1 nm and an objective lens defocus length of −10 nm, where the cations are imaged as two bright dots while oxygen ions show a dark contrast. This simulation further supports the refined structure of the CSZ-10.

The surface morphologies of $(\text{Ca}_{0.8}\text{Sr}_{0.2})\text{ZrO}_3$ ceramics sintered at 1,480 °C for 2–12 h are shown in Fig. 5a–f. The result indicated that an increase in sintering time has an effect on both grain morphology and shape. The grain size increased, the holes reduced and a mass of spheroid grains emerged as the sintering time increased from 2 to 6 h. With

further increasing time, the number of spheroid grains increased while that of octahedral grains decreased and finally disappeared when sintered for 10 h. As the sintering time is up to 12 h, holes increased exponentially.

MW measurements were performed as a function of sintering time whereas dielectric characteristics from 100 kHz up to 1 MHz were carried out on only ceramics sintered for 2 and 10 h. Figure 6a displays relative density and dielectric constant (ϵ_r) versus sintering time for $(\text{Ca}_{0.8}\text{Sr}_{0.2})\text{ZrO}_3$ ceramics. With increasing sintering time, the relative density of the specimen first increase and then decreased. The CSZ-10 sample with 10 h sintering had the maximum relative density of 95.1 %. According to Fig. 5, the growth of spheroid grains could facilitate the densification of the polycrystalline ceramics. An increase in number of holes should be responsible for the decreasing density of the CSZ-12 sample. Interestingly, the change trend of dielectric constant (ϵ_r) is consistent with that of relative density as sintering time increases. This suggests that the dielectric properties of the samples are closely related to their structural densification, and higher dielectric constant accompanies higher relative density. Among all samples, the CSZ-10 sample has the highest ϵ_r value of 27.9.

$Q \times f$ and τ_f values of variable-time sintering $(\text{Ca}_{0.8}\text{Sr}_{0.2})\text{ZrO}_3$ samples are shown in Fig. 6b. With increasing sintering time, the $Q \times f$ value first increases and then decreases, which is similar to the change-trend of the dielectric constant. Like ϵ_r , the CSZ-10 sample has the maximum $Q \times f$ value of 21,460 GHz (at 7.3 GHz). Often, the dielectric loss of microwave materials is contributed from both intrinsic and extrinsic components. Intrinsic loss is associated with lattice vibrational modes, whereas extrinsic loss is determined by impurities, dopants, grain boundaries, grain morphology and shape, secondary phase, pores, etc. [19, 20]. Like dielectric constant, the variation of $Q \times f$ value is similar to that of the relative density with increasing sintering time, and the $Q \times f$ values of the samples are also related to their relative density. Therefore, higher densification accompanying lower loss contributes to higher $Q \times f$ value. Clearly, the growth of different size spheroid grains in polycrystalline ceramics is helpful for the reduction of pores and the densification of ceramics. As a result, the highest $Q \times f$ value of 21,460 GHz is observed

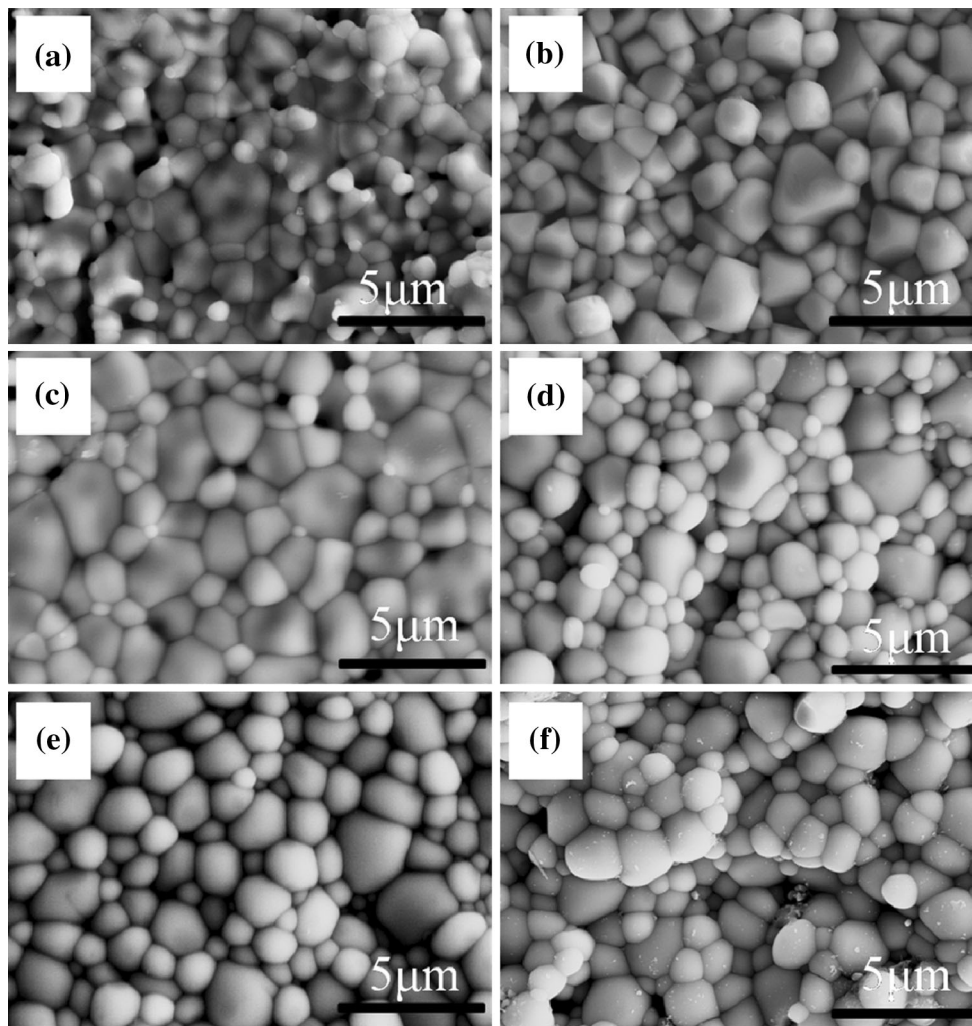


Fig. 5 SEM images of $(\text{Ca}_{0.8}\text{Sr}_{0.2})\text{ZrO}_3$ ceramics sintered at $1,480\text{ }^\circ\text{C}$ for **a** 2 h, **b** 4 h, **c** 6 h, **d** 8 h, **e** 10 h and **f** 12 h

in the CSZ-10 sample. It is well known that the τ_f value of microwave materials is contributed from their composition, the additions and the second phases in them. It can be seen that on obvious change in τ_f value of the samples is resulted from the increase of the sintering time, due to no significant compositional change or the presence of second phase. The τ_f value of the $(\text{Ca}_{0.8}\text{Sr}_{0.2})\text{ZrO}_3$ ceramics (2–12 h) changes from $+13.6$ to -14 ppm/ $^\circ\text{C}$.

Figure 7 shows the frequency dependence of dielectric properties for CSZ-2 and CSZ-10 at room temperature from 100 kHz up to 1 MHz. It can be seen that the dielectric constant and dielectric loss decreased with increasing frequency and sintering time. The decrease in ϵ_r can be explained by the reduction of the active polarization mechanism. At low frequencies, the electronic, ionic, dipolar, and interfacial/surface polarization contribute to the permittivity, whereas the mobile charges diffuse under the influence of an applied field up to the interface and build up the surface charge until the applied field reverses

with alternating voltage. However, at higher frequencies, these ionic motions are sensitive to the frequency and cannot follow the field variation. Hence, the contribution from the interfacial/surface polarization is minimized at higher frequencies, and therefore the permittivity decreased [21]. In the low frequency range, the majority conducting defects presumably follow the in direction of the applied electric field leading to a large leakage current and thereby giving rise to a higher dielectric loss. As frequency increases, this is no longer true. Hence dielectric loss tends to decreased with increasing frequency [22]. The porous ceramic (CSZ-2) is a typical lossy dielectric due to the loose structure, and has higher dielectric constant and higher dielectric loss in the low frequency range which is dominated by high electrical conductivity. Comparatively, The CSZ-10 sample has lower high-frequency dielectric constant and lower high-frequency dielectric loss due to its density structure. When the frequency increases close to 1 MHz, the dielectric loss and the dielectric constant of

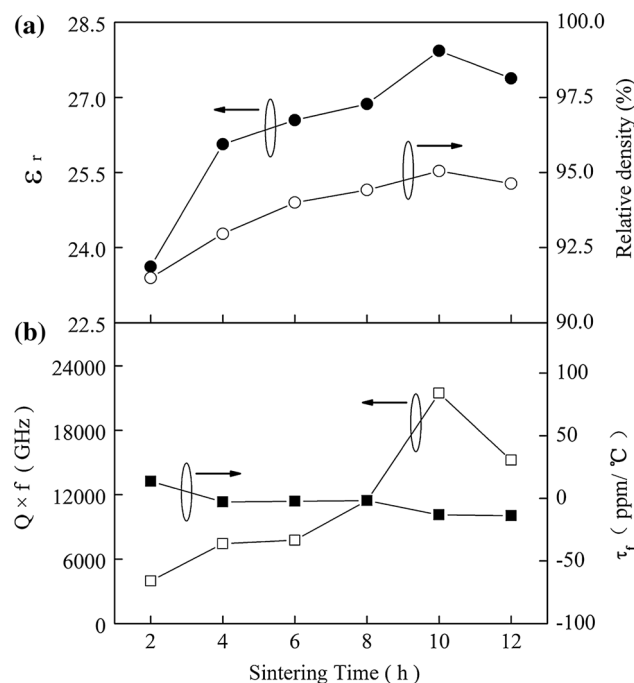


Fig. 6 Microwave dielectric properties: **a** relative density and dielectric constant (ϵ_r), **b** $Q \times f$ and τ_r values of $(\text{Ca}_{0.8}\text{Sr}_{0.2})\text{ZrO}_3$ ceramics sintered at 1,480 °C for 2–12 h

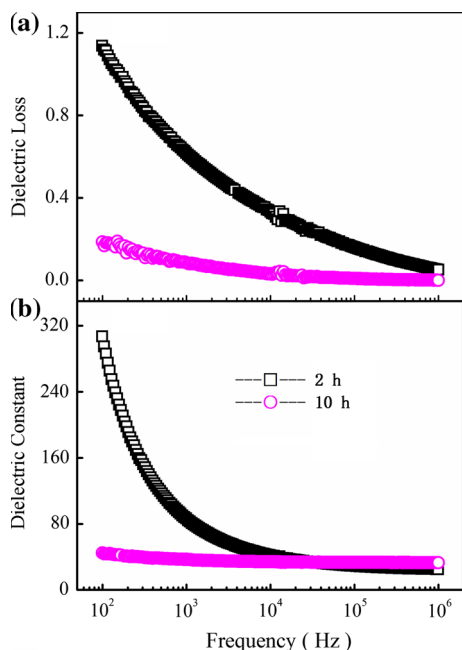


Fig. 7 Frequency dependence of dielectric properties for the CSZ-2 and CSZ-10 from 100 Hz to 1 MHz at room temperature

both the CSZ-2 and CSZ-10 converge at a reasonably small value (see Table 4).

Figure 8 shows the $\ln(\sigma)$ versus $1,000/T$ plots for all samples. Correspondingly, the activation energy (E_a) can be calculated from the Arrhenius equation:

Table 4 Dielectric constant and dielectric loss of CSZ-2 and CSZ-10 at various frequencies

| Frequency | CSZ-2 | | CSZ-10 | |
|-----------|--------------|---------------|--------------|---------------|
| | ϵ_r | $\tan \delta$ | ϵ_r | $\tan \delta$ |
| 0.1 kHz | 306.83 | 1.1357 | 44.72 | 0.18598 |
| 1 kHz | 86.27 | 0.6182 | 36.94 | 0.08625 |
| 10 kHz | 41.95 | 0.3328 | 33.94 | 0.03288 |
| 100 kHz | 28.76 | 0.1603 | 33.14 | 0.00947 |
| 1 MHz | 24.75 | 0.0515 | 32.94 | 0.000994 |
| 7.34 GHz | 23.62 | 0.0036 | 27.38 | 0.000341 |

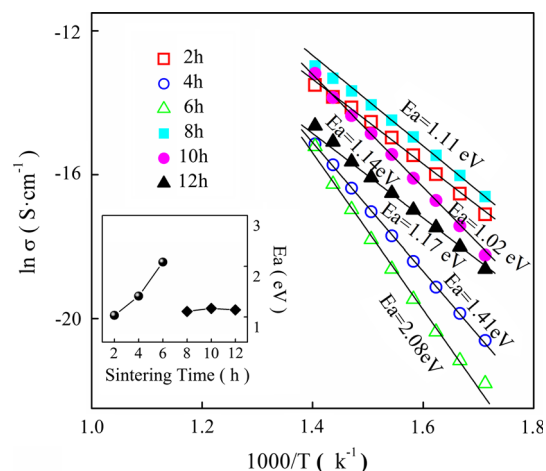


Fig. 8 Arrhenius plot of dc electrical conductivity (σ) of $(\text{Ca}_{0.8}\text{Sr}_{0.2})\text{ZrO}_3$ ceramics sintered at 1,480 °C for 2–12 h. Inset shows the trend of activation energy (E_a)

$$\sigma = A \cdot \exp(-E_a/kT) \quad (2)$$

where E_a is the nominal activation energy per charge carrier, k is Boltzmann's constant, and T is the absolute temperature. E_a can be estimated from the slope of the theoretical fitting lines (solid lines in Fig. 8), which is shown in the inset of Fig. 8. In the present work, the E_a values varied from 1.02 to 2.08 eV with various sintering time. Straumal et al. [23, 24] suggested that the effect of grain boundary is close related to the ferromagnetism of the ZnO films. Also, Hills et al. [25] reported that the electrolyte resistance of the CaZrO_3 ceramics is mainly controlled by the grain boundary. With increasing sintering time, the ceramics become denser and the grain boundary effect is enhanced. Hence, the E_a values increased and the conductivity decreased in the range of 2–6 h. However, further increasing time leads to a sharp increase in conductivity and a rapid decrease in E_a value. The E_a values are in the range from 1.11 to 1.17 eV which are close to those of the oxygen vacancy activation energy (1.005–1.093) [26]. It is likely that long time sintering at

high temperature causes the oxygen loss from lattice positions, and oxygen vacancies are mainly conduction species in the long-time sintering samples, associated with the following reaction:



Therefore, higher concentration oxygen vacancies result in higher conductivities and lower E_a values in the 8–12 h samples. The produced excess electrons accompanying the oxygen loss could give rise to the reduction of Zr ion, from Zr^{4+} to Zr^{3+} , which is similar to the $Ti^{4+} \rightarrow Ti^{3+}$ reduction [27]. Like $Ti^{4+} \rightarrow Ti^{3+}$, the instability of the oxidation state of Zr ion and the high ion-jump conduction of $Zr^{4+} \leftrightarrow Zr^{3+}$ further lead to the high conductivities and lower E_a values of the 8–12 h samples. Therefore, it is believed that the defect conduction and grain boundary effect together contribute to the non-trivial conduction behaviors of the $(Ca_{0.8}Sr_{0.2})ZrO_3$ ceramics.

4 Conclusions

Variable sintering time (2–12 h) $(Ca_{0.8}Sr_{0.2})ZrO_3$ ceramics were prepared by using a solid-state reaction process and their crystal structure and microwave dielectric properties were investigated in order to clarify the effect of sintering time. No change in crystal structure is induced due to the variance of sintering time. Rietveld refinement for the $(Ca_{0.8}Sr_{0.2})ZrO_3$ sintered for 10 h was carried out by using powder XRD at room temperature and it crystallizes in orthorhombic space group $Pnma$ [$a = 5.77341(4) \text{ \AA}$, $b = 8.05569(6) \text{ \AA}$, $c = 5.63318(4) \text{ \AA}$ and $V = 261.9920(30) \text{ \AA}^3$; $Z = 4$]. Interestingly, an increase in sintering time led to a significant impact on grain morphologies (changed from octahedral grains to spheroid grains), dc electrical conductivity and microwave dielectric properties.

Acknowledgments This work was supported by the National Natural Science Foundation (51172187), the SPDRF (20116102130002, 20116102120016) and 111 Program (B08040) of MOE, and Xi'an Science and Technology Foundation (XBCL-1-08, CX12174), and

Shaanxi Province Science Foundation (2013KW12-02), and the NPU Fundamental Research Foundation (NPU-FRF-JC201232) of China.

References

1. R.J. Cava, *J. Mater. Chem.* **11**, 54–62 (2001)
2. C.L. Huang, J.Y. Chen, *J. Alloy Compd.* **499**, 48–52 (2010)
3. X.L. Chen, H.F. Zhou, L. Fang, X.B. Liu, Y.L. Wang, *J. Alloys Compd.* **509**, 5829–5832 (2011)
4. Y.B. Chen, *J. Alloys Compd.* **478**, 657–660 (2009)
5. P.L. Wise, I.M. Reaney, W.E. Lee, T.J. Price, D.M. Iddles, *J. Eur. Ceram. Soc.* **21**, 2629–2632 (2001)
6. J.Y. Chen, C.L. Huang, *Mater. Lett.* **64**, 2585–2588 (2010)
7. N. Lamrani, B. Itaalit, S. Marinell, M. Aliouat, *Mater. Lett.* **65**, 346–369 (2011)
8. H. Stetson, B. Schwartz, *J. Am. Ceram. Soc.* **44**, 420–421 (1961)
9. B.W. Hakki, P.D. Coleman, *IEEE Trans. Microwave Theory Tech.* **8**, 402–410 (1960)
10. W.E. Courtney, *IEEE Trans. Microwave Theory Tech.* **18**, 476–485 (1970)
11. V.M. Orera, C. Pecharroman, J.I. Pena, R.I. Merino, C.J. Serna, *J. Phys. Condens. Matter* **10**, 7501–7510 (1998)
12. C.H. Perry, D.J. McCarthy, G. Rupprecht, *Phys. Rev.* **138**, A1537–A1538 (1965)
13. H. Zheng, I.M. Reaney, *J. Mater. Res.* **19**, 488–495 (2004)
14. A.C. Larson, R.B. Von Dreele, LANL Rep. LAUR **86**, 748 (1994)
15. B.H. Toby, *J. Appl. Crystallogr.* **34**, 210–213 (2001)
16. R.I. Smith, A.R. West, *J. Solid State Chem.* **108**, 29–36 (1994)
17. R.D. Shannon, *Acta Crystallogr. A* **A32**, 751–767 (1976)
18. P. Stadelmann, *Java Version. 3.0505W2006*, 2006
19. H. Tamura, *Am. Ceram. Soc. Bull.* **73**, 92–95 (1994)
20. W. Wolfram, *Curr. Opin. Solid State Mater. Sci.* **1**, 715–731 (1996)
21. X.Y. Chen, S.X. Baia, M. Li, W.J. Zhang, *J. Eur. Ceram. Soc.* **33**, 3001–3006 (2013)
22. V. Ting, Y. Liu, L. Nore'n, R.L. Withers, D.J. Goossens, M. James, C. Ferraris, *J. Solid State Chem.* **177**, 4428–4442 (2004)
23. B.B. Straumal, A.A. Mazilkin, S.G. Protasova, P.B. Straumal, A.A. Myatiev, G. Schütz, E. Goering, T. Tietze, B. Baretzky, *Philos. Mag.* **93**(10–12), 1371–1383 (2013)
24. B.B. Straumal, S.G. Protasova, A.A. Mazilkin, G. Schütz, E. Goering, B. Baretzky, P.B. Straumal, *JETP Lett.* **97**, 415–426 (2013)
25. M.P. Hills, C. Schwandt, R.V. Kumar, *J. Electrochem. Soc.* **153**, H189–H194 (2006)
26. S.C. Hwang, G.M. Choi, *J. Eur. Ceram. Soc.* **25**, 2609–2612 (2005)
27. N.D. Patil, P.S. Jadhav, R.N. Jadhav, S.N. Mathad, V. Puri, *Int. J. Self Propag. High Temp Synth.* **22**, 141–146 (2013)